



Insights into aerosol chemistry during the 2015 China Victory Day parade: results from simultaneous measurements at ground level and 260 m in Beijing

Jian Zhao^{1,3}, Wei Du^{1,3}, Yingjie Zhang^{4,1}, Qingqing Wang¹, Chen Chen¹, Weiqi Xu^{1,3}, Tingting Han^{1,3}, Yuying Wang⁵, Pingqing Fu¹, Zifa Wang¹, Zhanqing Li⁵, and Yele Sun^{1,2,3}

¹State Key Laboratory of Atmospheric Boundary Layer Physics and Atmospheric Chemistry, Institute of Atmospheric Physics, Chinese Academy of Sciences, Beijing 100029, China

²Center for Excellence in Urban Atmospheric Environment, Institute of Urban Environment, Chinese Academy of Sciences, Xiamen 361021, China

³College of Earth Sciences, University of Chinese Academy of Sciences, Beijing 100049, China

⁴Collaborative Innovation Center on Forecast and Evaluation of Meteorological Disasters, Nanjing University of Information Science & Technology, Nanjing 210044, China

⁵College of Global Change and Earth System Science, Beijing Normal University, Beijing 100875, China

Correspondence to: Yele Sun (sunyele@mail.iap.ac.cn)

Received: 2 August 2016 – Discussion started: 8 September 2016

Revised: 5 December 2016 – Accepted: 11 February 2017 – Published: 3 March 2017

Abstract. Strict emission controls were implemented in Beijing and adjacent provinces to ensure good air quality during the 2015 China Victory Day parade. Here, we conducted synchronous measurements of submicron aerosols (PM₁) at ground level and 260 m on a meteorological tower by using a high-resolution aerosol mass spectrometer and an aerosol chemical speciation monitor, respectively, in Beijing from 22 August to 30 September. Our results showed that the average PM₁ concentrations are 19.3 and 14.8 μg m⁻³ at ground level and 260 m, respectively, during the control period (20 August–3 September), which are 57 and 50 % lower than those after the control period (4–30 September). Organic aerosols (OAs) dominated PM₁ during the control period at both ground level and 260 m (55 and 53 %, respectively), while their contribution showed substantial decreases (~40 %) associated with an increase in secondary inorganic aerosols (SIAs) after the parade, indicating a larger impact of emission controls on SIA than OA. Positive matrix factorization of OA further illustrated that primary OA (POA) showed similar decreases as secondary OA (SOA) at both ground level (40 % vs. 42 %) and 260 m (35 % vs. 36 %). However, we also observed significant changes in SOA composition at ground level. While the more oxidized SOA showed a

large decrease by 75 %, the less oxidized SOA was comparable during (5.6 μg m⁻³) and after the control periods (6.5 μg m⁻³). Our results demonstrated that the changes in meteorological conditions and PM loadings have affected SOA formation mechanisms, and the photochemical production of fresh SOA was more important during the control period. By isolating the influences of meteorological conditions and footprint regions in polluted episodes, we found that regional emission controls on average reduced PM levels by 44–45 %, and the reductions were close among SIA, SOA and POA at 260 m, whereas primary species showed relatively more reductions (55–67 %) than secondary aerosol species (33–44 %) at ground level.

1 Introduction

Beijing, the capital of China, with ~21.71 million people in the metropolitan area (Beijing Municipal Bureau of Statistics, http://www.bjstats.gov.cn/tjsj/yjdsj/rk/2015/201603/t20160317_339143.html), has been suffering from severe air pollution during the past decade (Sun et al., 2006, 2012, 2016; Chan and Yao, 2008; Huang et al., 2014;

Guo et al., 2014; R. Zhang et al., 2015). According to the Beijing Environmental Statement, the annual average mass concentration of fine particles ($\text{PM}_{2.5}$) in Beijing is $80.6 \mu\text{g m}^{-3}$ in 2015, which was decreased by 6.2 % compared with that in 2014. However, the concentration was more than twice the China National Ambient Air Quality Standard ($35 \mu\text{g m}^{-3}$ as an annual average), suggesting that air pollution in Beijing is still severe. For these reasons, extensive studies utilizing various offline and online techniques have been conducted to investigate the characteristics of aerosol particles and the formation mechanisms of haze episodes (Zhao et al., 2013; Tian et al., 2014; Elser et al., 2016). Among them, the Aerodyne Aerosol Mass Spectrometer (AMS) is unique, as it is capable of getting size-resolved chemical information of non-refractory submicron aerosols (NR- PM_1) in real time (DeCarlo et al., 2006; Canagaratna et al., 2007). While the research-grade AMS has been widely used in air pollution studies in China (Sun et al., 2010; Huang et al., 2010; Huang et al., 2011; Xu et al., 2015; Hu et al., 2016b), the deployments of the compact and robust aerosol chemical speciation monitor (ACSM) (Ng et al., 2011) are relatively new (Sun et al., 2012; Y. J. Zhang et al., 2015; Li et al., 2016). Together, these studies have significantly improved our understanding of the composition, processes and sources of submicron aerosols (PM_1). For example, long-term monitoring results showed that organics contributed the largest fraction of PM_1 (40–51 %) during all seasons in urban Beijing, followed by nitrate (17–25 %) and sulfate (12–17 %) (Y. L. Sun et al., 2015). Positive matrix factorization analysis further highlighted substantial different organic aerosols (OAs) composition in different seasons. Generally, secondary OA (SOA) is the major component of OA in summer, on average, accounting for 57–64 % (Huang et al., 2010; Sun et al., 2010, 2012; J. K. Zhang et al., 2015), while primary OA (POA) made a higher contribution in winter and even as much as ~ 70 %, especially with the significantly enhanced coal combustion OA in heating seasons (Liu et al., 2011; Y. L. Sun et al., 2013; Hu et al., 2016a). Back-trajectory analysis showed that high PM_1 mass concentrations were often associated with air masses from the south and southwest, and the composition was characterized by high fractions of oxidized OA and secondary inorganic aerosols (SIAs are a combination of sulfate, nitrate and ammonium), whereas primary species emitted from local sources were the dominant contributors during clean events (Huang et al., 2010; Sun et al., 2010, 2012; Zhang et al., 2015a). In addition, the impacts of meteorological parameters (e.g., temperature, relative humidity) on the formation and evolution of pollution events in winter were also extensively studied (Y. Sun et al., 2013; Y. L. Sun et al., 2013; Zhang et al., 2014; Wang et al., 2015; Jiang et al., 2015). Results showed that stagnant meteorological conditions, local emissions, regional transport and secondary production were four major factors leading to the formation of severe haze episodes in Beijing in winter (Sun et al., 2014; Zhang et al., 2014; Liu et al., 2016).

However, most previous studies were conducted at the ground sites which are subject to strong influences from local sources, e.g., traffic and cooking emissions. The mixed local emissions increase the difficulties in quantifying the relative contributions of local sources and regional transport to severe haze pollution. Despite this, real-time characterization of submicron aerosols at high altitudes in the megacity of Beijing is rare. Y. Sun et al. (2015) conducted the first real-time measurements of PM_1 at 260 m on a meteorological tower using an ACSM along with synchronous measurements at the ground site by an Aerodyne high-resolution time-of-flight AMS (HR-AMS hereafter). While secondary aerosol species had similar temporal variations between 260 m and the ground site, the variations in primary species were substantially different. In addition, a relatively higher contribution of nitrate was observed at 260 m (15 %) than at the ground site (10 %), which was likely due to the enhanced gas–particle partitioning associated with lower temperature and higher relative humidity (RH) at 260 m. Chen et al. (2015) further found that the variations in primary and secondary aerosol species were similar at 260 m, while they were significantly different at the ground site. These results illustrated a significant impact of regional transport on aerosol species at high altitudes. However, due to the limited synchronous studies at ground level and high altitude in the city, our knowledge of the sources and evolutionary processes of aerosol particles, particularly in different seasons with different meteorological conditions, is far from complete.

Understanding of the relationship between source emissions and aerosol chemistry is of great importance for mitigating air pollution in megacities. For example, strict emission controls were often implemented in Beijing and the surrounding regions to ensure good air quality during specific events, e.g., the Beijing Olympic Games in 2008 and the Asia-Pacific Economic Cooperation (APEC) summit in 2014, which offered experimental opportunities to study the impacts of source emission controls on air pollution. Huang et al. (2010) found that strict emission controls along with favorable meteorological conditions led to the low PM_1 levels during the Beijing Olympic Games. Similarly, all PM_1 species at 260 m were observed to decrease substantially (40–80 %) as a response to strict emission controls over a regional scale during APEC (Chen et al., 2015). In contrast, secondary species showed substantial reductions at ground level, ranging from 35 to 69 %, yet the reductions in primary species were much smaller (Xu et al., 2015). These studies highlight the importance of regional emission controls in decreasing secondary aerosol precursors, and hence suppressing the formation of secondary aerosols, yet a more strict local emission control is also needed. To ensure good air quality during the 2015 China Victory Day parade, a series of temporary control measures were implemented in Beijing and the surrounding regions from 20 August to 3 September. These strict emission controls included stopping construc-

tion activities, restricting the number of vehicles by alternating odd and even plate numbers, prohibiting outdoor barbecues and shutting down factories and power plants in adjacent provinces. Such measures were even stricter than those during APEC by extending control areas to the Shandong province. As a consequence, the air quality hit the best record since the release of the PM_{2.5} standard in 2012, leading to 15 blue-sky days, which was commonly referred to “Parade Blue”. The average PM_{2.5} concentration was 18 $\mu\text{g m}^{-3}$ during the control period (http://www.gov.cn/xinwen/2015-09/07/content_2926447.htm), which was decreased by 73.1 % during the same period in 2014. In addition, the PM levels and meteorological conditions were both significantly different from those during the 2014 APEC summit. Thus, this study period is unique in investigating aerosol characteristics during low-PM-level periods and further evaluating the impacts of emission controls on aerosol sources, composition and processes.

Here, we deployed an HR-AMS and an ACSM at ground level and 260 m, respectively, for synchronous measurements of aerosol particle composition, including organics (Org), sulfate (SO₄), nitrate (NO₃), ammonium (NH₄) and chloride (Chl) from 22 August to 30 September 2015, along with collocated measurements of black carbon (BC) and size-resolved number concentrations. The mass concentrations, chemical composition and diurnal variations of submicron aerosol species at ground level and 260 m during and after the control period were characterized and compared. The sources of OA at different heights were investigated by positive matrix factorization and the changes in OA composition due to emission controls were elucidated. In addition, the sources of aerosol particle species during and after the control period were investigated with FLEXPART analysis and bivariate polar analysis.

2 Experimental methods

2.1 Sampling site and meteorology

The sampling site is located at the tower branch of the Institute of Atmospheric Physics (IAP), CAS (39°58′28″ N, 116°22′16″ E; 49 m.a.s.l.), which is a typical urban site that is subject to influences from local traffic and cooking emissions nearby (Y. L. Sun et al., 2015). The detailed information about this sampling site was presented in previous studies (Sun et al., 2012; Y. L. Sun et al., 2015). The meteorological parameters including temperature (*T*), RH and winds (wind speed and wind direction) were obtained from the Beijing 325 m meteorological tower at 15 heights (8, 15, 32, 47, 65, 80, 100, 120, 140, 160, 180, 200, 240, 280 and 320 m). While the average RH, *T* and wind speed were relatively similar between the control (20 August–3 September) and non-control periods (4 September–30 September) (Table 1), the prevailing winds were substantially different. The control period

was characterized by dominant northerly winds while the non-control period showed both the northerly and southerly prevailing winds (Fig. S1 in the Supplement). All the data in this study were reported at ambient pressure and temperature in Beijing Time (i.e., Coordinated Universal Time +8 h).

2.2 Instrumentation and operation

The HR-AMS and ACSM were deployed at ground level and 260 m, respectively, for synchronous measurement of NR-PM₁ species from 22 August to 30 September 2015. The HR-AMS was situated in a sampling room located at the rooftop of a two-story building (~8 m). The ambient air was drawn into the sampling room through a stainless steel tube with the flow rate of 10 L min⁻¹ of which ~0.085 L min⁻¹ was isokinetically sampled into the HR-AMS. Coarse particles with aerodynamic diameters larger than 2.5 μm were removed by a PM_{2.5} URG cyclone (URG-2000-30ED) that was mounted in front of the sampling line. A silica gel diffusion dryer was also set up in front of the inlet system to avoid water vapor condensation which reduces the uncertainties in particle collection efficiency (CE) due to variable humidity (Matthew et al., 2008). Mass spectrum (MS) and particle time-of-flight (PToF) modes were cycled every ~10 s in mass-sensitive V mode to obtain mass concentrations and size distributions with a time resolution of 5 min. The high-mass-resolution W mode (5 min) was also operated for subsequent high-resolution spectral analysis and elemental analysis. The calibrations of HR-AMS were conducted following the standard protocols described in previous publications (Jayne et al., 2000; Jimenez, 2003).

Collocated instruments at the ground site included a two-wavelength aethalometer (AE22, Magee Scientific Corp.) for BC (880 nm), a cavity-attenuated phase shift extinction monitor (CAPS PM_{ext}, Aerodyne Research Inc.) for light extinction ($\lambda = 630 \text{ nm}$) of dry fine particles and a CAPS NO₂ monitor (Aerodyne Research Inc.) for gaseous NO₂. Gas analyzers (Thermo Scientific) for O₃, CO, NO and NO_y, and a tapered element oscillating microbalance (TEOM series 1400a, Thermo Scientific) for PM_{2.5} were also deployed on the roof of another two-story building, which was located approximately 30 m to the north. In addition, a tandem differential mobility analyzer (TDMA) that is developed by the Guangzhou Institute of Tropical and Marine, China Meteorological Administration, was used to measure size-resolved particle number concentrations between 10 and 400 nm. A detailed description of the TDMA system is presented elsewhere (Tan et al., 2013).

The ACSM and collocated instruments were stored in two containers at 260 m on the tower. The measurements included NR-PM₁ species by the ACSM, particle number concentrations (15–600 nm) by a scanning mobility particle sizer (SMPS) that was equipped with a long differential mobility analyzer (DMA 3082L, TSI) and a condensation particle counter (CPC 3775, TSI), BC (880 nm) by a seven-

Table 1. Summary of average meteorological parameters and chemical compositions during and after the control period, and the entire study at ground level and 260 m. Change percentages in mass concentrations of PM₁ species during and after the control period are also shown.

	260 m				Ground			
	Entire	Control period	Non-control period	Change perc. (%)	Entire	Control period	Non-control period	Change perc. (%)
Meteorological parameters								
<i>T</i> (°C)	21.01	23.40	19.94		22.77	25.50	21.55	
RH (%)	66.36	65.73	66.64		62.66	60.18	63.76	
WS (m s ⁻¹)	4.07	4.03	4.08		1.22	1.28	1.20	
Aerosol species (µg m ⁻³)								
Org	10.82	7.77	12.03	35.4	15.96	10.71	18.31	41.5
POA	3.77	2.72	4.18	34.7	5.51	3.78	6.34	40.4
HOA					1.69	0.89	2.07	57.0
COA					3.83	2.89	4.26	32.2
SOA	7.05	5.04	7.85	35.8	10.45	6.93	11.97	42.1
LO-OOA					6.21	5.57	6.48	14.0
MO-OOA					4.24	1.36	5.49	75.2
SO ₄	3.87	2.19	4.54	51.8	7.37	3.39	9.09	62.8
NO ₃	5.28	2.26	6.47	65.0	7.16	2.37	9.23	74.3
NH ₄	2.74	1.38	3.29	58.1	4.36	1.63	5.53	70.5
Chl	0.34	0.13	0.42	69.5	0.37	0.07	0.51	87.1
BC	2.42	1.04	3.02	65.5	2.22	1.17	2.71	56.6
PM ₁	25.47	14.76	29.76	50.4	37.44	19.34	45.38	57.4

wavelength aethalometer (AE33, Magee Scientific Corp.), and scattering and extinction coefficients of dry fine particles at 630 nm by a CAPS single-scattering albedo monitor (CAPS PM_{ssa}, Aerodyne Research Inc.). The sampling setup and operations at 260 m were overall similar to those at the ground site. Before the deployments, the ACSM measurements were first compared with those of HR-AMS at the ground site. All submicron aerosol species measured by the ACSM were highly correlated with those measured by the HR-AMS ($r^2 > 0.97$), and the regression slopes of ACSM against HR-AMS varied from 0.61 to 1.24 for different aerosol species. Therefore, the ACSM measurements were further corrected using the regression slopes from the intercomparisons. More details are given in Y. Sun et al. (2015). In addition, a 3-day intercomparison between AE22 and AE33 was performed after the campaign. As shown in Fig. S2, BC measured by AE22 was highly correlated with that measured by AE33 ($r^2 = 0.99$), yet a systematic underestimation by 28% was also observed. Thus, BC measured by AE22 at ground level was further corrected by dividing a factor of 0.72 for a better comparison with that measured by AE33 at 260 m.

2.3 Data analysis

The high-resolution mass spectra of HR-AMS were analyzed using the standard ToF-AMS data analysis software packages (SQUIRREL v. 1.57H and PIKA

v. 1.16H, <http://cires1.colorado.edu/jimenez-group/ToFAMSResources/ToFSoftware/index.html>) and the ACSM data were analyzed for the mass concentrations using the standard data analysis software (v. 1.5.3.0). The default relative ionization efficiency (RIE) values were used for NO₃, SO₄, Chl and Org, except for NH₄, which was determined from pure NH₄NO₃ particles during IE calibration.

CE was introduced to correct the incomplete detection of submicron particles by the HR-AMS and ACSM (Zhang et al., 2005) which depends on several particle and ambient air properties, including particle acidity, ammonium nitrate fraction and relative humidity (Matthew et al., 2008; Middlebrook et al., 2012). In this study, aerosol particles were almost neutralized at both ground level and 260 m (Fig. S3). The average mass fraction of NH₄NO₃ was 19.4 and 18.3% at 260 m and the ground site, respectively, indicating that NH₄NO₃ would not affect CE substantially. In addition, aerosol particles were dried before sampling into the inlet system. Thus, CE = 0.5 was used for both the HR-AMS and ACSM data analysis. Further validations of CE by comparison with collocated measurements are given in Sect. 3.1.

The elemental composition of OA, including oxygen-to-carbon (O/C), hydrogen-to-carbon (H/C), nitrogen-to-carbon (N/C) and organic-mass-to-organic-carbon (OM/OC) ratios, was determined with the “improved-ambient” (I-A) method (Canagaratna et al., 2015), which

was revised recently on the basis of previous “Aiken-ambient” (A-A) method (Aiken et al., 2007, 2008). Note that the O/C and H/C ratios derived from the I-A method are on average 27 and 9 %, respectively, larger than those from the A-A method (Fig. S4).

Positive matrix factorization (PMF) with the PMF2.exe (v4.2) algorithm (Paatero and Tapper, 1994) was used to analyze the HR-AMS and ACSM organic spectral matrices following the procedures reported in Ulbrich et al. (2009). The detailed data pretreatment and PMF evaluations were the same as those reported in Chen et al. (2015) and Xu et al. (2015). Two factors, including a hydrocarbon-like OA (HOA) and an oxygenated OA (OOA), were identified at 260 m, while four factors, including a HOA, a cooking-related OA (COA), a more oxidized OOA (MO-OOA) and a less oxidized OOA (LO-OOA), were resolved at the ground site due to the improved sensitivity and chemical resolution of the HR-AMS. These OA factors were distinguished by their unique signatures in mass spectral patterns and diurnal variations. The correlations between OA factors and specific external tracers and also other diagnostic plots were given in the Supplement (Figs. S5–S8).

2.4 Estimation of particle density

The number concentrations from SMPS measurements were converted to mass concentrations using the composition-dependent density (Fig. 1a) that was estimated with the measured submicron aerosol composition assuming spherical particles in Eq. (1) (Aiken et al., 2009; Salcedo et al., 2006):

$$\rho_{\text{comp}} = \frac{[\text{NO}_3^-] + [\text{SO}_4^{2-}] + [\text{NH}_4^+] + [\text{Cl}^-] + [\text{BC}] + [\text{Org}]}{\frac{[\text{NO}_3^-] + [\text{SO}_4^{2-}] + [\text{NH}_4^+]}{1.75} + \frac{[\text{Cl}^-]}{1.52} + \frac{[\text{BC}]}{1.77} + \frac{[\text{Org}]}{1.2}}, \quad (1)$$

where the densities are 1.75 g cm^{-3} for ammonium nitrate and ammonium sulfate, 1.52 g cm^{-3} for ammonium chloride (Lide, 1991), 1.2 g cm^{-3} for organic aerosols (Turpin and Lim, 2001) and 1.77 g cm^{-3} for BC (Park et al., 2004; Poulain et al., 2014).

2.5 Source region analysis

The footprints of aerosol particles during specific events were calculated using the Lagrangian particle dispersion model FLEXPART (Stohl et al., 2005). In this study, the meteorological field was simulated by the Weather Research and Forecasting (WRF) model (Skamarock et al., 2005) with a time resolution of 1 h and spatial resolution of 10 km. In the simulations, 2-day backward trajectories and 10 000 tracer particles were calculated at a height of 50 m during five polluted episodes and two clean periods to investigate the potential source regions of aerosol particles. In addition, the potential source regions of PM_{10} species during control and non-control periods at 260 m were investigated using bivariate polar plots (Carslaw and Ropkins, 2012). Compared

with FLEXPART analysis, bivariate polar plots depending on wind speed and wind direction are subject to offer more insights into the sources of aerosol species over a small scale.

3 Results and discussion

3.1 Intercomparisons

As indicated in Fig. 1, PM_{10} (the combination of NR- PM_{10} and BC) overall tracked well with collocated measurements from the SMPS, TEOM and CAPS with R^2 ranging from 0.84 to 0.94. The mass concentrations derived from the SMPS measurements on average accounted for 45 % of PM_{10} , mainly due to the different size cutoff (e.g., 10–400 nm for SMPS). On average, PM_{10} contributed 81 % of $\text{PM}_{2.5}$, which indicates that submicron aerosol accounted for a large fraction of $\text{PM}_{2.5}$ in Beijing. Note that this value is slightly higher than that obtained during previous studies conducted in urban Beijing (64–77 %) (Sun et al., 2012; Zhang et al., 2014; Y. L. Sun et al., 2015). One explanation is that BC was included in the comparisons. In addition, the light extinction of fine particles was tightly correlated with PM_{10} at the ground site ($R^2 = 0.92$) as well, and the mass extinction coefficient of $\text{PM}_{2.5}$ was also consistent with previous observations in Beijing (Han et al., 2015).

The collocated measurements at 260 m were also correlated well with each other ($R^2 = 0.76$ – 0.94 ; Fig. S9). The PM_{10} measured by the ACSM and AE33 showed an excellent agreement with that (15–600 nm) derived from the SMPS measurements ($R^2 = 0.92$, slope = 0.91; Fig. S10c). We also compared the PM_{10} with SMPS mass concentrations that converted from 15 to 400 nm particles at both of these two heights (Fig. S9a and b). A higher ratio of 0.69 was observed at 260 m than that at ground (0.45). This difference might suggest higher contributions of aerosol particles with mobility diameters below 400 nm at 260 m than at the ground site. The detailed discussions of the differences in size distributions and particle number concentrations between 260 m and the ground site will be presented elsewhere (Du et al., 2017).

3.2 Mass concentrations and chemical composition

The time series of PM_{10} and meteorological parameters at two different heights during the entire study are shown in Fig. 2. The PM_{10} concentrations remained consistently low, generally less than $50 \mu\text{g m}^{-3}$ during the control period, while episodes with PM_{10} concentrations higher than $50 \mu\text{g m}^{-3}$ were frequently observed after the control period. On average, the mass concentrations of PM_{10} are 19.3 and $14.8 \mu\text{g m}^{-3}$ at ground level and 260 m, respectively, during the control period, which were decreased by 57 and 50 % compared to those after the control period (Table 1). The average mass concentration of PM_{10} at ground level during the control period was significantly lower than that during other periods with strict emission controls, for example,

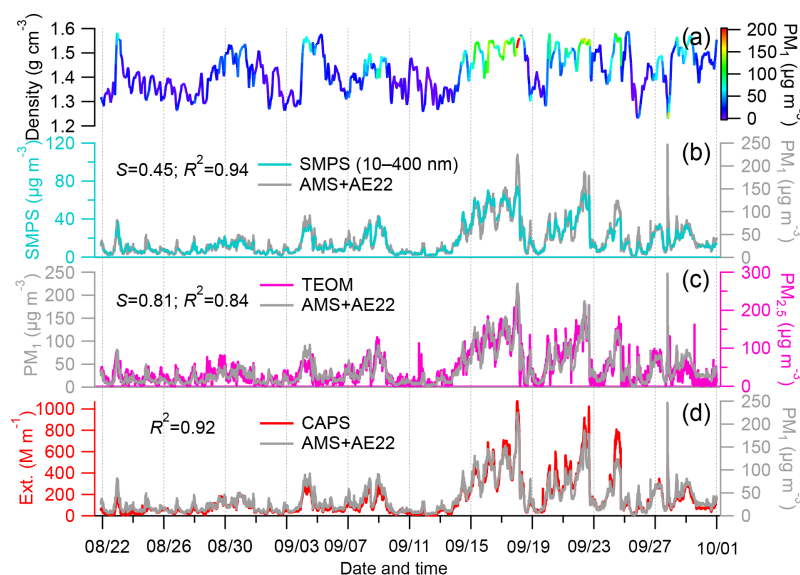


Figure 1. (a) Time series of particle density and intercomparisons between PM_{10} (the combination of NR-PM_{10} and BC) and (b) mass concentrations derived from SMPS measurements, (c) $\text{PM}_{2.5}$ and (d) the light extinction coefficient of $\text{PM}_{2.5}$. The correlation coefficients (R^2) and regression slopes (S) are also given in (b–d).

$63.1 \mu\text{g m}^{-3}$ during Beijing 2008 Olympics Games (Huang et al., 2010) and $41.6 \mu\text{g m}^{-3}$ during 2014 APEC summit (Xu et al., 2015). These results indicate a significantly improved air quality during the parade period. Inorganic species (e.g., sulfate, nitrate and chloride) during the control period were 63–87 % lower than those measured after the control period, while organics had a relatively smaller decrease by 42 %. The decreases of aerosol species during the parade were substantially larger than those during APEC (e.g., 41–69 % for inorganic species and 35 % for organics) (Xu et al., 2015), likely due to more strict emission controls and the favorable northerly winds (Fig. S2a). Although the average PM_{10} concentration ($11.3 \mu\text{g m}^{-3}$) measured by an ACSM at Tsinghua University, approximately 5 km northwest of our sampling site, during the same period is relatively lower than that in this study, the reductions in total PM_{10} (63.5 %), inorganic species (65–78 %) and organics (53 %) were consistent (Li et al., 2016). Compared to ground level, the average PM_{10} concentration at 260 m was also lower than that measured at 260 m during the 2014 APEC summit ($24.1 \mu\text{g m}^{-3}$) (Chen et al., 2015). The PM_{10} species were also decreased substantially during the control period, which are 52–69 % for inorganic species and 35 % for OA. Note that aerosol reductions at ground level were overall larger than those at 260 m (Table 1), indicating that local and regional emission controls might affect ground level and 260 m differently.

The average composition of PM_{10} at ground level and 260 m during and after the control period is shown in Fig. 2. Aerosol composition was overall similar at the two heights during the control period, which was dominated both by organics (53–55 %) followed by sulfate (15–18 %) and nitrate

(12–15 %). After the control period, aerosol composition had significant changes, particularly for OA and nitrate. For instance, the OA contribution decreased from 53–55 to 40 % while the nitrate contribution increased from 12–15 to 20–22 %. Such compositional changes were overall similar to those observed during APEC. One explanation is that regional emission controls have a large impact on the reduction of secondary aerosols by decreasing their precursors and suppressing secondary formation, while strong local OA sources, e.g., cooking activities, still exist during the control period (Xu et al., 2015). We also observed higher nitrate contributions at 260 m and higher sulfate contributions at ground level. Indeed, the average ratio of $\text{NO}_3 / \text{SO}_4$ at ground (0.92) was lower than that obtained at 260 m (1.29). Similar vertical differences were reported in previous studies in Beijing, which were likely caused by the enhanced nighttime nitrate formation at high altitude associated with high O_3 (Brown and Stutz, 2012), and the favorable gas–particle partitioning of nitrate due to low T at 260 m (Y. Sun et al., 2015; Chen et al., 2015). These results also demonstrate that different sources and formation mechanisms can affect the vertical distributions of nitrate and sulfate (Y. Sun et al., 2015).

3.3 OA composition and sources

Four OA factors including two primary factors (HOA and COA) and two secondary factors (LO-OOA and MO-OOA) were identified at the ground site. The HOA mass spectrum was primarily composed of hydrocarbon ions of $\text{C}_n\text{H}_{2n-1}^+$ and $\text{C}_n\text{H}_{2n+1}^+$ (Fig. 3a) that are common characteristics of primary combustion emissions, e.g., diesel and gasoline ex-

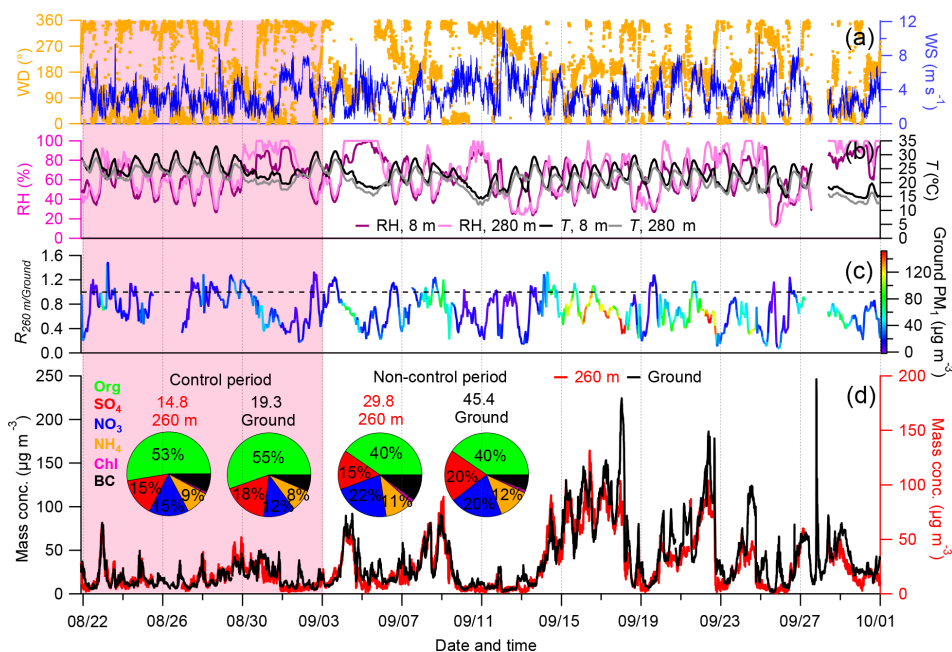


Figure 2. Time series of (a) wind direction (WD) and wind speed (WS) at 280 m, (b) relative humidity (RH) and temperature (T), (c) ratio of 260 m to ground for PM₁ and (d) PM₁ mass concentrations at 260 m and ground. The pie charts depict the average chemical composition during and after the control period at 260 m and the ground site, respectively.

haust (Canagaratna et al., 2004; Lanz et al., 2007; Mohr et al., 2009). The O/C ratio of HOA (0.23; I-A method) was higher than the values (0.15–0.17; A-A method) reported in previous studies in Beijing (Huang et al., 2010; Xu et al., 2015) and Shanghai (Huang et al., 2012). HOA was well correlated with BC ($R^2 = 0.71$) during the entire study. Note that HOA was correlated with BC during both the control period ($R^2 = 0.69$) and non-control period ($R^2 = 0.58$), and the ratio of HOA/BC was also similar (0.74 vs. 0.69). These results indicate that HOA has similar sources to BC at the ground site, and the emission controls did not affect HOA/BC ratio significantly. Indeed, the concentrations of HOA and BC decreased similarly by $\sim 57\%$ during the control period.

The COA mass spectrum is characterized by the high m/z 55/57 ratio and also has a similar O/C ratio (0.13; I-A method) to those (0.08–0.13; A-A method) from traditional Chinese cooking emissions (He et al., 2010). COA was correlated with the marker ion $C_6H_{10}O^+$ ($R^2 = 0.95$) and showed a pronounced diurnal cycle with two prominent peaks occurring at lunch and dinner times, consistent with the observations from many previous studies (Huang et al., 2010; Sun et al., 2011; Xu et al., 2014). Although the average COA concentration during the control period ($2.89 \mu\text{g m}^{-3}$) was 32% lower than that after the control period ($4.26 \mu\text{g m}^{-3}$), the variations and concentrations of most COA peaks were similar between control and non-control periods (Fig. 3b). These results indicate the presence of local cooking emissions despite regional emission controls. Considering that COA con-

tributed a comparable fraction of OA, which is 27 and 23% during the control and non-control periods, respectively, a stricter control of local cooking emissions is needed to further improve air quality in urban Beijing.

The two OOA factors were both dominated by prominent m/z 44 yet with different O/C ratios. The O/C ratio of MO-OOA is 1.0, which is much higher than that of LO-OOA (0.84). In addition, MO-OOA showed a much higher f_{44} (mass fraction of m/z 44 in OA) and m/z 44/43 ratio than LO-OOA. All these results indicate that MO-OOA was more oxidized than LO-OOA. Consistently, MO-OOA was better correlated with sulfate compared with LO-OOA ($R^2 = 0.86$ vs. 0.64) during this study. The fact that LO-OOA was weakly correlated with nitrate during control and non-control periods suggested very different formation mechanisms between these two species. The temporal variations of MO-OOA and LO-OOA were substantially different. As shown in Fig. 3, MO-OOA showed ubiquitously lower concentration during the control period than non-control period. On average, the MO-OOA concentration is $1.36 \mu\text{g m}^{-3}$ during the control period, which is decreased by 75% compared to that after the control period. In contrast, LO-OOA showed comparable concentrations during and after the control period, with the average concentration being 5.57 and $6.48 \mu\text{g m}^{-3}$. Our results showed that SOA was dominated by less oxidized OA during the control period while highly oxidized OA was more important after the control period. One explanation is that regional emission controls slowed down the aging pro-

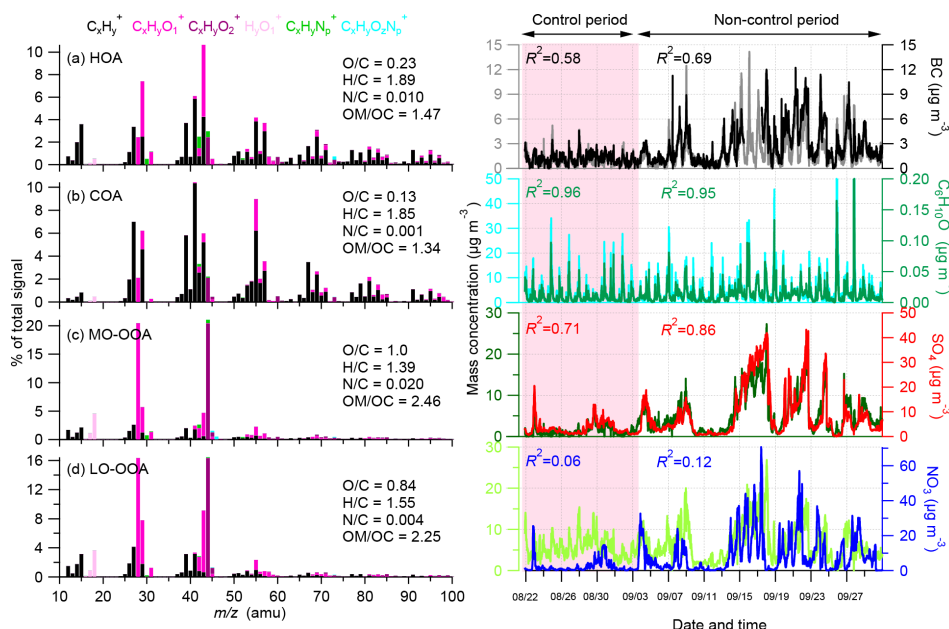


Figure 3. High-resolution mass spectra (left panel) and time series (right panel) of four OA factors at the ground site: (a) hydrocarbon-like OA (HOA), (b) cooking-related OA (COA), (c) more oxidized oxygenated OA (MO-OOA) and (d) less oxidized OOA (LO-OOA). The time series of BC, sulfate and nitrate are shown for comparisons, and the correlation coefficients (R^2) between OA factors and external tracers during the control (pink area) and non-control periods are also shown. The elemental ratios in the left panel were calculated from the I-A method (Canagaratna et al., 2015).

cesses of OA by decreasing its precursors of volatile organic compounds (VOCs) and O_3 levels.

Compared to the ground site, two OA factors, i.e., HOA and OOA, were identified at 260 m (Fig. 4), mainly due to low mass resolution and sensitivity of the ACSM. The mass spectral profiles of these two OA factors were similar to those identified at 260 m before and during APEC (Sun et al., 2015a; Chen et al., 2015). High m/z 55/57 and noticeable m/z 60, a marker for biomass burning in the spectrum, likely indicate that HOA is a factor mixed with multiple primary emissions, e.g., traffic, biomass burning and cooking. HOA was tightly correlated with BC during the non-control period ($R^2 = 0.70$), whereas the correlation was much weaker during the control period ($R^2 = 0.30$). Similarly stronger correlations during the non-control period were also observed between OOA and secondary inorganic species (Fig. 4). Such differences in correlations likely indicate that regional emission controls have changed the variations in BC, OA and inorganic species at higher altitudes while those at ground sites were less affected.

Overall, the composition of OA was dominated by SOA at both the ground site and 260 m during the entire study, on average accounting for 65 % (Fig. 5). The average mass concentrations of SOA and POA are $7.10 \mu\text{g m}^{-3}$ and $3.79 \mu\text{g m}^{-3}$, respectively, at 260 m, which was 32.5 and 31.6 % lower than those at the ground site. Although the temporal variations of SOA were similar ($R^2 = 0.64$ and 0.77 during and after the control period, respectively) between

ground level and 260 m, POA showed more dramatic differences between these two heights ($R^2 = 0.17$ and 0.15 during and after the control period, respectively). One explanation is that SOA was more influenced by the formation over regional scales, while the vertical differences in POA were more sensitive to various local primary source emissions, including cooking, traffic and biomass burning. The fact that the diurnal variations of POA varied more dramatically at the ground site than 260 m supported that the ground site is more subject to influences from local sources compared with 260 m (Chen et al., 2015). Indeed, POA was even correlated with SOA at 260 m ($R^2 = 0.69$) and the diurnal OA composition was relatively stable throughout the day, indicating that primary and secondary species were more well mixed at higher altitudes due to a dominant source from regional transport. Although the contributions of POA and SOA to OA remained small changes during and after control periods at the ground site and 260 m, SOA composition at the ground site had significant changes. While the contribution of LO-OOA to OA was decreased from 52 % during the control period to 35 % after the control period, that of MO-OOA was increased from 13 to 30 %. These changes in SOA composition illustrated the importance of fresh SOA during clean periods, while aged SOA was more important during polluted episodes. Further studies are needed to investigate how emission controls and meteorological differences affect the transformations between LO-OOA and MO-OOA.

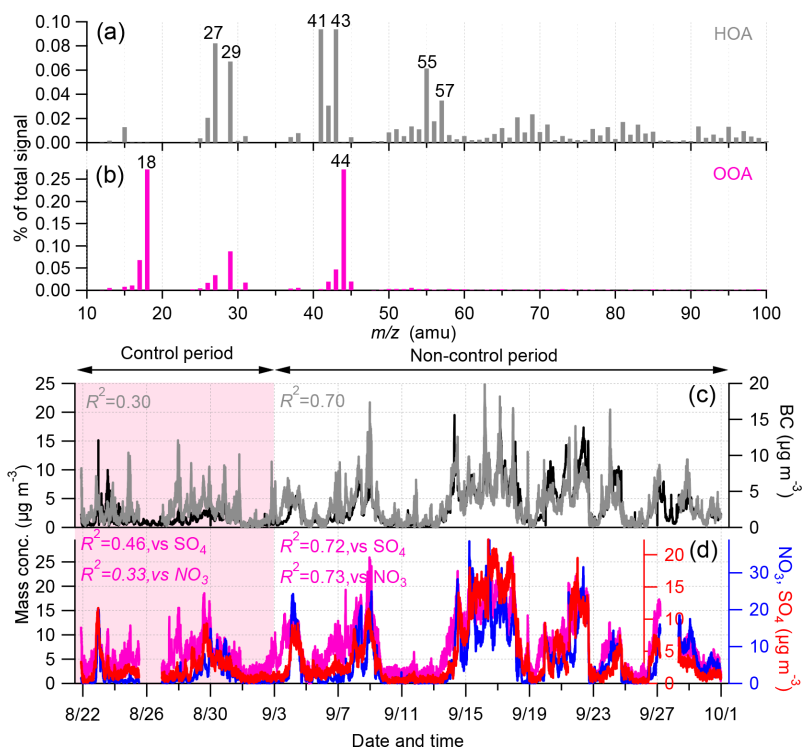


Figure 4. Mass spectral profiles and time series of (a, c) hydrocarbon-like OA (HOA) and (b, d) oxygenated OA (OOA) at 260 m. Also shown are the time series of BC, sulfate and nitrate for comparisons. The correlation coefficients (R^2) between OA factors and external tracers during control (pink area) and non-control periods are also given in panels (c) and (d).

3.4 Aerosol chemistry differences between ground level and 260 m

As indicated in Fig. 2c, the ratio of 260 m to ground ($R_{260\text{ m}/\text{Ground}}$) for PM_{10} was less than 1 for most of the time, which indicated that the PM_{10} level at 260 m was overall lower than that at ground level. Indeed, NR- PM_{10} species measured at 260 m were 35–53 % lower than those at ground level (Fig. S11). Although PM_{10} species showed similar variations between the two heights ($R^2 = 0.59\text{--}0.80$), periods with largely different concentrations were also observed, particularly during the periods with high PM_{10} levels (Fig. 6). Figure 7 depicts that $R_{260\text{ m}/\text{Ground}}$ showed a gradual decrease as a function of PM loadings ($> 60\ \mu\text{g m}^{-3}$) for most aerosol species, e.g., sulfate, nitrate and ammonium, indicating larger vertical gradients during more polluted episodes. For example, the $R_{260\text{ m}/\text{Ground}}$ of nitrate was approximately 0.88 below $90\ \mu\text{g m}^{-3}$ and then rapidly decreased to 0.28 when PM_{10} increased to $210\ \mu\text{g m}^{-3}$. Also note that the $R_{260\text{ m}/\text{Ground}}$ were substantially different for each species. Sulfate showed the lowest $R_{260\text{ m}/\text{Ground}}$ among all aerosol species during the same PM levels. One reason is the different sources at different heights. Another reason is the different formation mechanisms associated with different meteorological parameters, e.g., RH, T and solar radiation, and also the different size distributions at the two

heights. POA showed a largely different vertical variation from SOA. Previous studies showed overall higher POA concentrations at ground level due to the influences from local source emissions (Y. Sun et al., 2015). However, POA at 260 m was comparable with that at ground level in this study. One reason is that POA at 260 m was mixed with part of SOA due to the limitation of PMF analysis of ACSM spectra. This is supported by the similar variations between POA and SOA at 260 m ($R^2 = 0.69$). BC is a clear exception showing an increasing trend in $R_{260\text{ m}/\text{Ground}}$ as a function of PM loadings. The reason is not clear yet, but could be due to more aged BC at 260 m from regional transport while local BC emissions were not significant. For example, diesel trucks and heavy-duty vehicles are not allowed inside the city during daytime. Figure 7 also showed a large variation in $R_{260\text{ m}/\text{Ground}}$ during periods with low PM loadings (e.g., $< 30\ \mu\text{g m}^{-3}$) as indicated by the range of 25th and 75th percentiles. This result indicates that the vertical differences between ground level and 260 m during clean periods are subject to multiple influences and can vary substantially. In addition, the evolution of the mixing layer could be another factor that influences $R_{260\text{ m}/\text{Ground}}$. As shown in Fig. S12, almost all aerosol species showed clear diurnal patterns with lower $R_{260\text{ m}/\text{Ground}}$ values during nighttime and in the early morning and higher values during the afternoon. Sulfate, however, showed a much smaller variation in diurnal

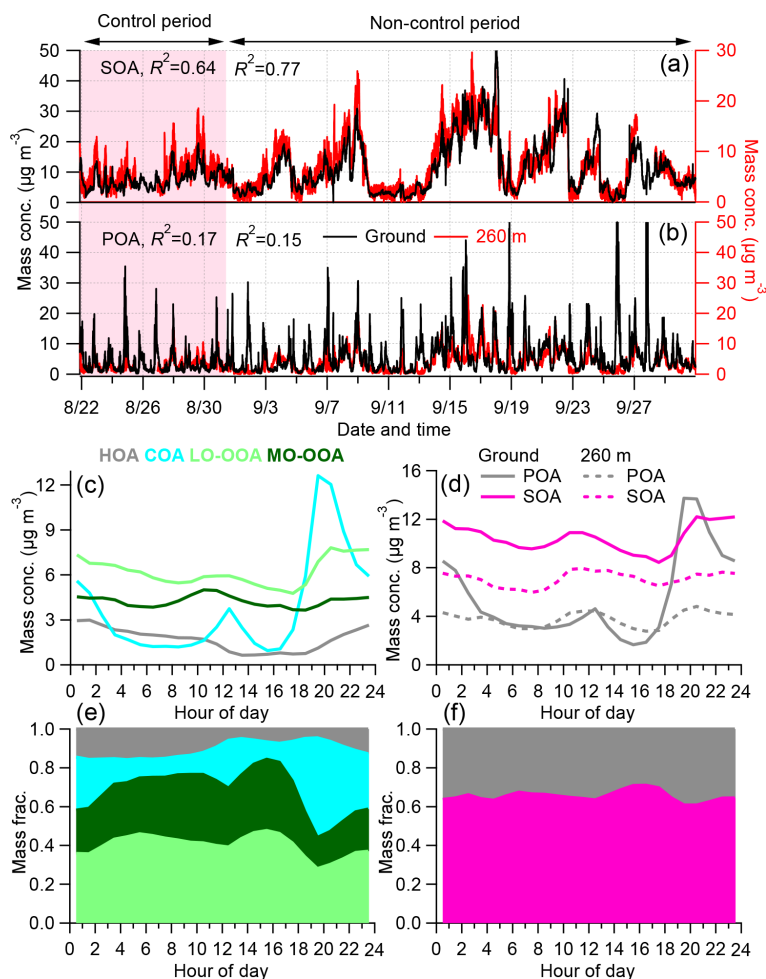


Figure 5. (a, b) A comparison of time series of SOA and POA at ground and 260 m, (c) diurnal variations of four OA factors at the ground site, (d) diurnal variations of POA and SOA at the ground site and 260 m and (e–f) the diurnal mass fractions of OA factors in (c) at ground and (d) at 260 m.

nal cycle of $R_{260\text{ m}/\text{Ground}}$, consistent with the fact that sulfate was formed over a regional scale and relatively well mixed.

3.5 Diurnal evolution of aerosol species

The diurnal variations of PM_{10} species during and after the control periods at ground level and 260 m are depicted in Fig. 8. While the diurnal patterns between the two heights were overall similar, we also observed large vertical differences, particularly during nighttime. For example, POA in OA showed much larger vertical differences during nighttime than daytime due to enhanced cooking emissions and shallow boundary layer. As a comparison, such differences were much reduced during daytime due to a stronger vertical mixing associated with elevated boundary layer height.

SOA showed similar diurnal variations between the two heights, yet the diurnal variations were quite different during and after the control period. SOA showed a pronounced noon peak during the control period, indicating the impor-

tance of photochemical processing in driving the diurnal evolution of SOA. This also explained the dominance of photochemically processed LO-OOA in SOA during the control period. In contrast, the diurnal cycle of SOA was relatively flat after the control period, likely indicating that SOA was more aged over a regional scale, which is consistent with the dominance of highly oxidized MO-OOA in SOA. The diurnal variations of POA and SOA together led to a strong diurnal cycle of organics at ground level and 260 m, which was characterized by two pronounced peaks at noon and nighttime. The diurnal cycle of sulfate was remarkably similar between ground level and 260 m. This is consistent with the fact that sulfate is mainly formed over a regional scale, and the contribution of local photochemical production is generally small (Salcedo et al., 2006; Sun et al., 2011). The diurnal cycle of BC, a tracer of combustion emissions, varied differently from secondary aerosol species, but was generally characterized by high concentrations during nighttime (Han et al., 2009; Huang et al., 2010). As shown in Fig. 8h, BC

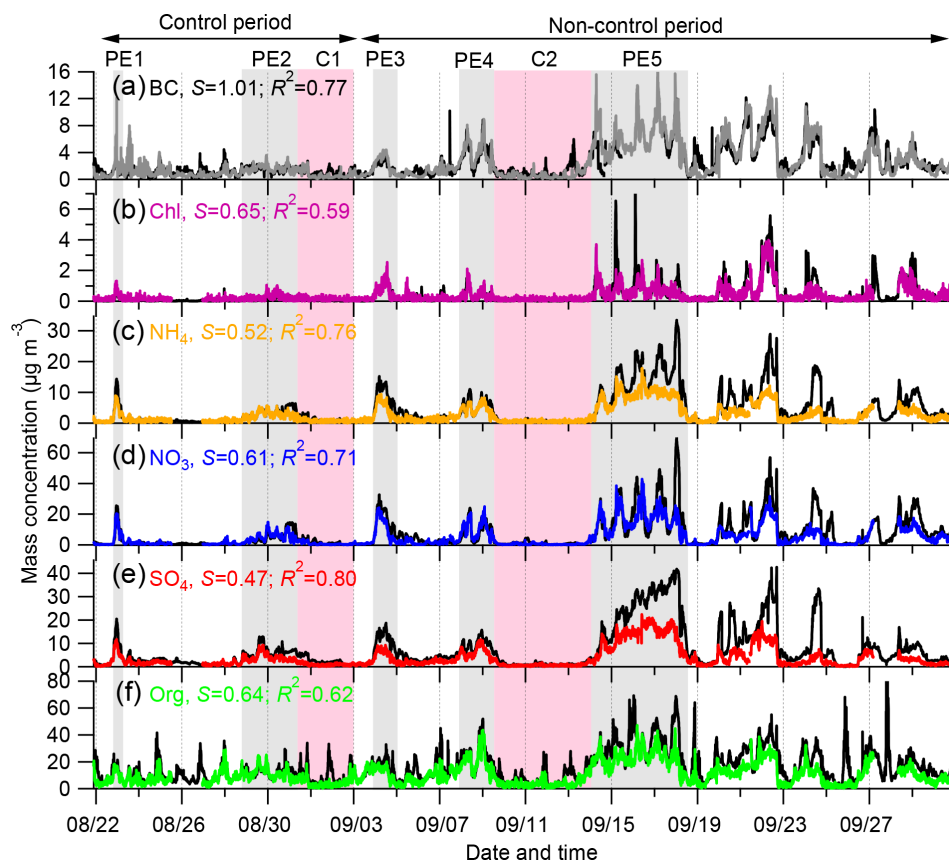


Figure 6. Comparisons of the time series of aerosol species between the ground site (black lines) and 260 m (colored lines). Five pollution episodes (PE1, PE2, PE3, PE4 and PE5) and two clean periods (C1 and C2) are marked for further discussions.

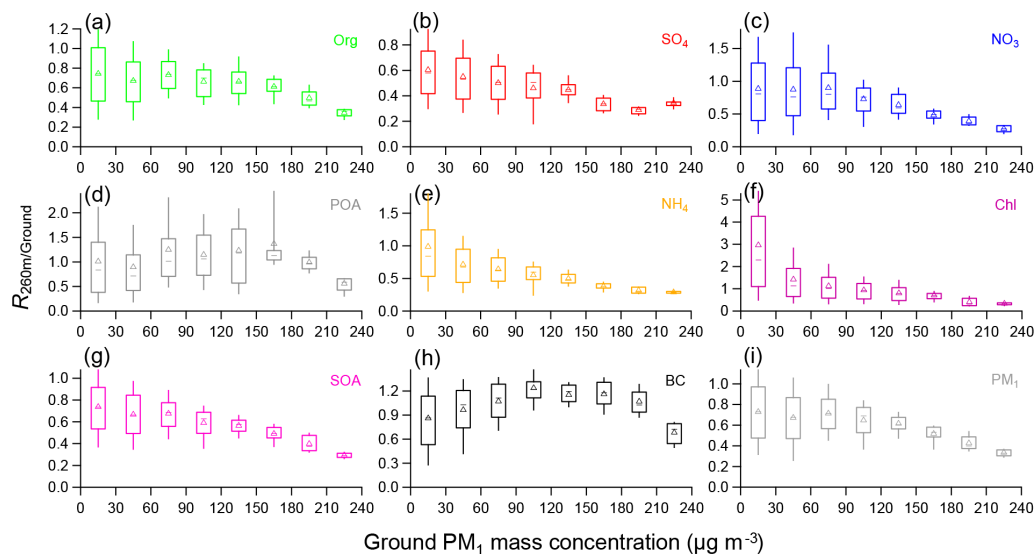


Figure 7. Variations of the ratios of 260 m to ground ($R_{260\text{m}/\text{Ground}}$) for each species as a function of PM_{10} mass concentrations at ground level. The data are grouped into eight bins according to PM_{10} loadings ($30\ \mu\text{g m}^{-3}$ increments). The median (middle horizontal lines), mean (triangles), 25th and 75th percentiles (bottom and top boxes) and 10th and 90th percentiles (bottom and top whiskers) are shown for each bin.

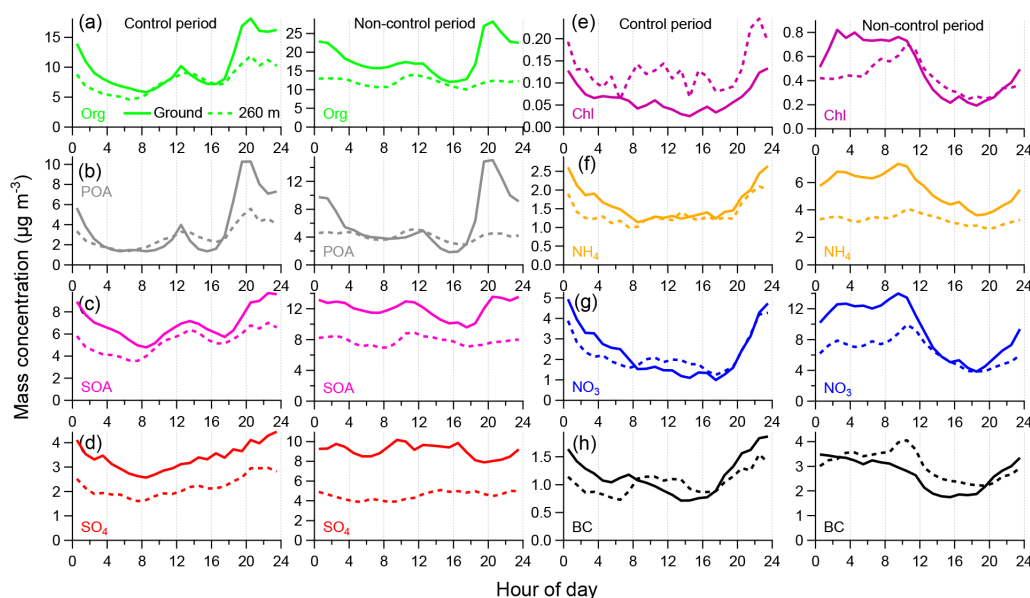


Figure 8. Diurnal variations of PM₁ species at ground level (solid lines) and 260 m (dash lines) during the control and non-control periods.

showed higher concentrations at the ground site than 260 m during nighttime during the control period, while this was reversed during daytime. One explanation is that BC came dominantly from local diesel trucks and heavy-duty vehicle emissions during nighttime, which can cause a clear vertical gradient due to the weaker vertical convection. In contrast, BC at 260 m was generally higher than that at the ground site during non-control period. This likely indicates an important source of BC coming from regional transport (Wang et al., 2016).

Ammonium, nitrate and chloride showed similar diurnal patterns at ground level and 260 m. However, the diurnal patterns were substantially different during and after the control period, indicating the changes in either sources or formation mechanisms. During the control period, these three species showed much higher concentrations during nighttime than daytime, suggesting a dominant impact of temperature-dependent gas–particle partitioning on diurnal variations, although the variations in boundary layer height also played a role. Note that chloride presented higher concentrations at 260 m than the ground site during the control period. One reason is likely due to the uncertainties in ACSM measurements because the concentrations were close to 5 min detection limits ($0.07 \mu\text{g m}^{-3}$ (Sun et al., 2012)). After the control period, these three species presented the highest concentrations from midnight to 10:00 BT at both the ground site and 260 m, and then rapidly decreased to low levels during the late afternoon. Such diurnal behaviors were similar to those previously observed in Beijing (Huang et al., 2010; Sun et al., 2012), which were mainly driven by temperature-dependent gas–particle partitioning. Vertically, the differences between the ground site and 260 m were the largest from midnight

to early morning, while they were almost disappeared in the afternoon due to strong vertical mixing.

3.6 Potential sources of aerosol species

Bivariate polar plots were used to explore potential source regions of submicron aerosol species at 260 m during control and non-control periods (Carslaw and Ropkins, 2012). As shown in Fig. 9a, high mass concentrations of aerosol species were mainly located in regions to the south and southeast of the observation site, highlighting an important role of regional transport to relatively high PM levels during the control period. Moreover, the center of bivariate polar plots with low wind speeds showed ubiquitously low concentrations, suggesting the absence of stagnant meteorological conditions in accumulation of pollutants during the control period. We also noticed different source regions for different aerosol species. For example, the source regions of BC, chloride, nitrate and ammonium were mainly located to the southeast, while POA, SOA and sulfate were from both the south and southeast. These results also indicate that regional emission controls likely changed aerosol composition substantially to the south and southeast of Beijing.

The potential source regions of aerosol species after the control period (Fig. 9b) were quite different from those during the control period. Most aerosol species showed high concentrations in the regions to the south, indicating the importance of regional transport in the formation of haze episodes. BC, chloride and POA, however, also showed high concentrations in areas with low wind speed, likely suggesting a considerable contribution of local source emissions under stagnant meteorological conditions. Our results have significant implications that air-pollution-mitigating strategies

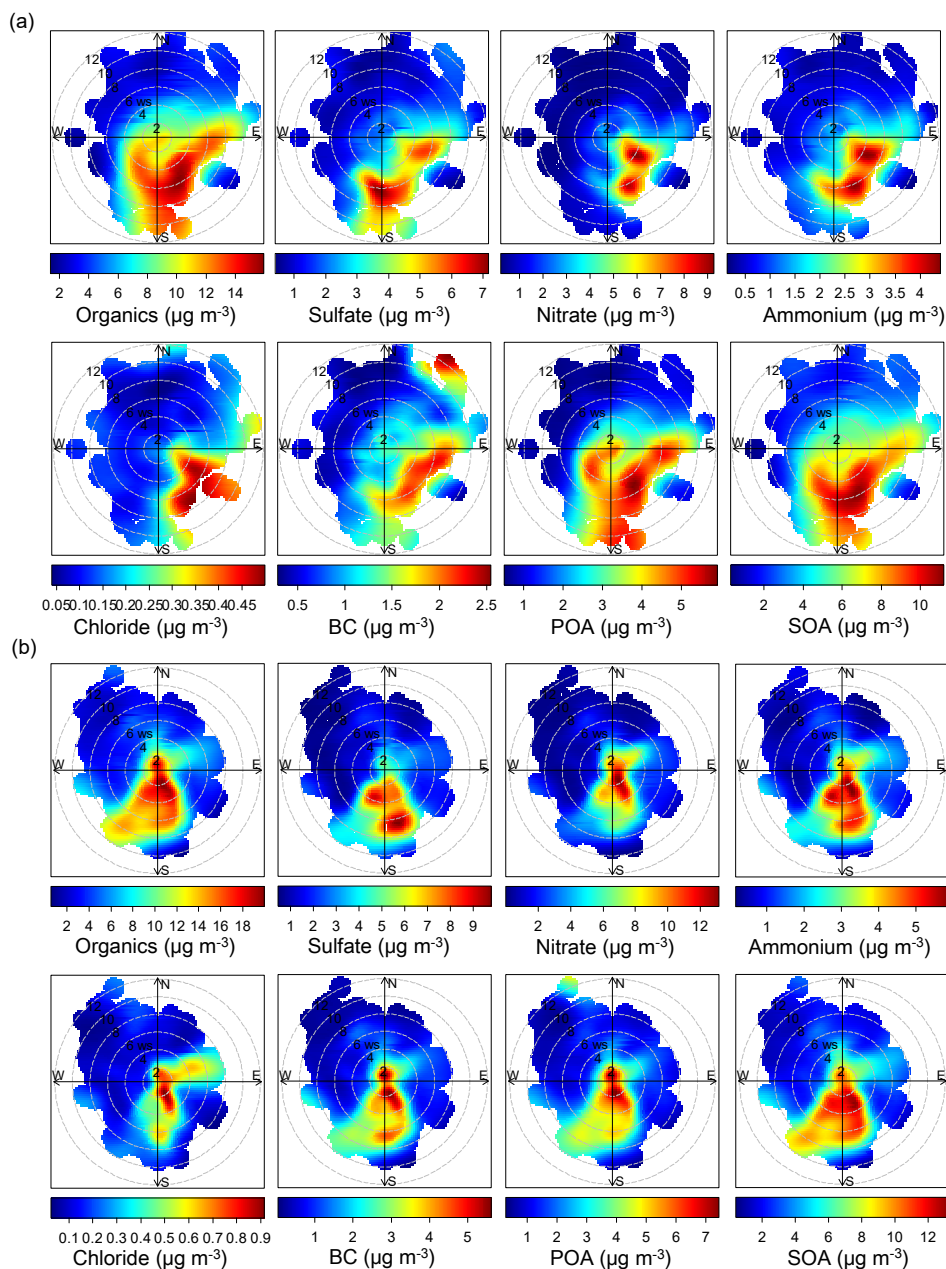


Figure 9. Bivariate polar plots of PM_{10} species during the (a) control and (b) non-control periods at 260 m as functions of wind direction and wind speed (m s^{-1}).

should focus on emission controls in regions to the south and southeast of Beijing while strict local emission controls are also needed to reduce primary species.

3.7 Case studies to investigate the effects of emission controls

Five polluted episodes and two clean periods (Fig. 6) were selected to better investigate the impacts of emission controls on aerosol chemistry during the control period. The two clean periods, C1 and C2, showed similar footprint regions

(Fig. 10) that were dominantly from the northeast. However, the average mass concentrations of PM_{10} during the control period (C1) were even higher, by 33 and 22 % at ground level and 260 m, respectively, than those after the control period (C2; Table S1 in the Supplement). We note that RH during C1 was much higher than that during C2 due to the influence of a precipitation event before C1. Therefore, higher mass concentrations during C1 were likely due to higher RH that facilitated the formation of secondary aerosols. In fact, the mass concentrations of SIA during C1 were 1.4–1.5 and 1.6–

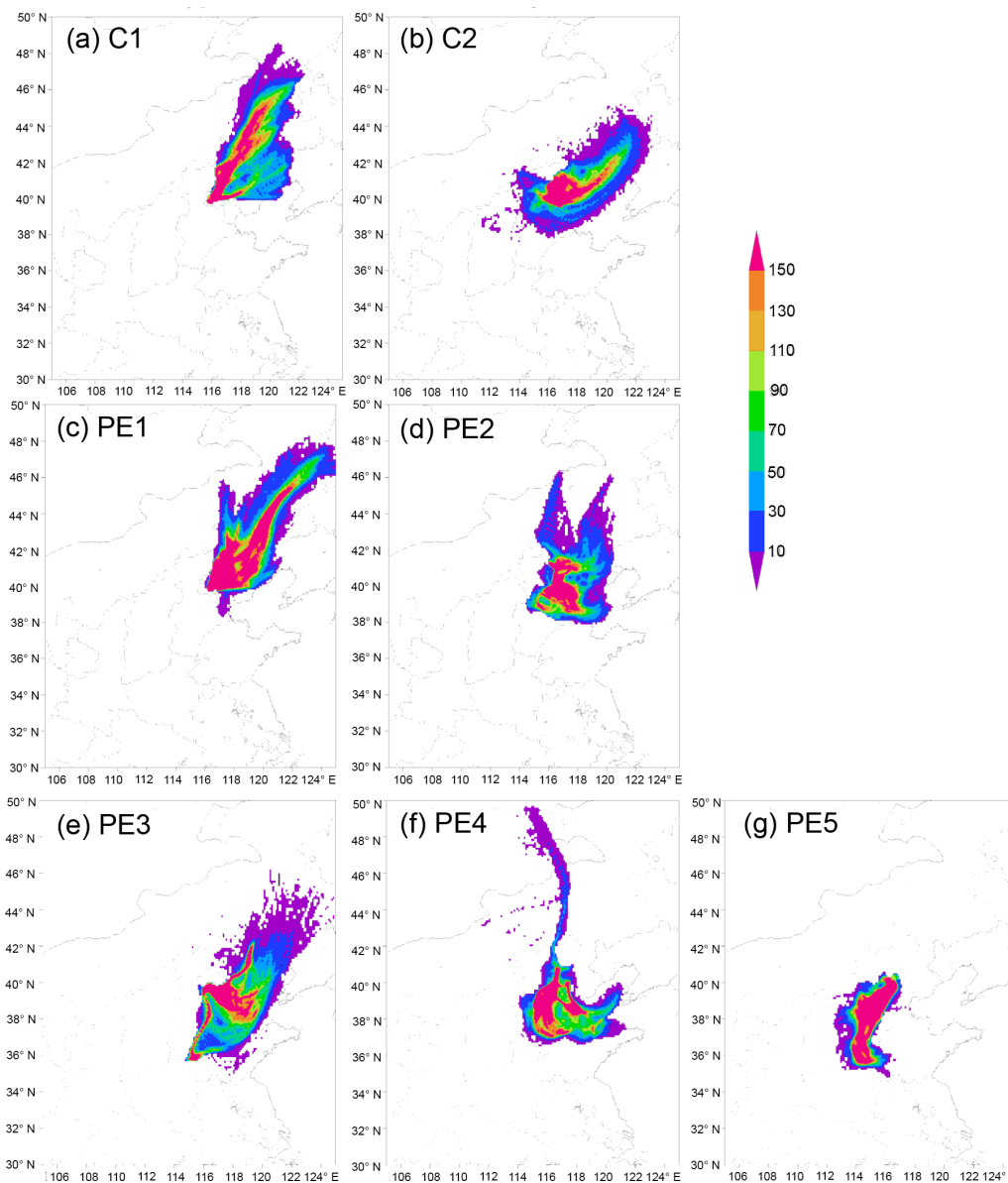


Figure 10. Footprint regions of two clean periods and five pollution episodes that are marked in Fig. 6. The color bar indicates the number concentrations of tracer particles.

2.1 times higher at 260 m and ground level, respectively, than those during C2, whereas primary species, e.g., BC and POA, were relatively close between C1 and C2 by varying less than 10%. Our results indicate that regional emission controls during parade appeared to have small impacts on clean periods for two reasons: (1) the air masses during clean periods are generally from the relatively clean regions with low anthropogenic emissions in the northwest and northeast, and (2) regional emission controls were mainly implemented in the regions to the south and southeast, e.g., the Hebei, Tianjin and Shandong provinces.

The footprint regions varied differently among the five polluted episodes, but generally from the south and south-

east except PE1 (Fig. 10). The two episodes, PE1 and PE2, during the control period showed substantially different composition which was likely due to the different source regions given their relatively similar meteorological conditions (Table S1). The average mass concentration of PM₁ during PE1 was ~40% higher than that during PE2 at both ground level and 260 m. While the PM₁ during PE1 was mainly composed of SIA (65 and 59% at ground level and 260 m, respectively), it was characterized by higher contribution of organics (44 and 47% at ground level and 260 m, respectively) during PE2. These results suggest that aerosol composition and concentrations during the control period can have significant differences during polluted episodes from different source re-

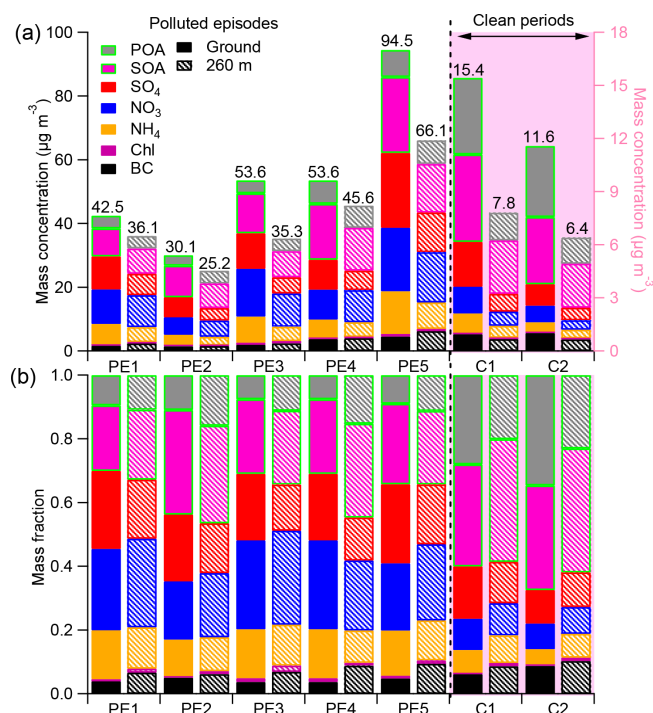


Figure 11. Average composition of PM₁: (a) mass concentrations and (b) mass fraction during the five polluted episodes (PE1, PE2, PE3, PE4 and PE5) and two clean periods (C1 and C2) at 260 m and at ground level.

gions. The mass concentrations of PM₁ varied more dramatically during three polluted episodes after the control period. While the average PM₁ mass concentration was close between PE3 and PE4, it was significantly lower than that during PE5. By comparison with PE1 and PE2 during the control period, we found that PE4 showed the most similar footprint region to PE2, and also the meteorological conditions between PE4 and PE2 were relatively similar. Therefore, the comparisons between PE2 and PE4 would be the best case to illustrate the impacts of emission controls in the south on PM levels and aerosol composition during the parade. The average PM₁ concentration was 30.1 and 25.2 $\mu\text{g m}^{-3}$ at ground level and 260 m, respectively, during PE2, which was reduced by 44–45 % compared with that during PE4. Furthermore, we observed remarkably similar composition of PM₁ and OA at 260 m between PE2 and PE4, which comprised 46 % SIA and 66 % SOA, respectively. This finding is consistent with our previous studies that regional emission controls can reduce PM levels substantially but have small impacts in changing the bulk composition due to the synergistic controls of aerosol precursors (Chen et al., 2015). In contrast, aerosol composition was slightly different between PE2 and PE4 at ground level. Primary species, e.g., BC, Chl and POA, showed relatively more reductions (55–67 %) than secondary aerosol species (33–44 %), indicating that local

emission controls also played a role in reducing the PM levels at ground sites.

4 Conclusions

An HR-AMS and an ACSM were deployed at ground level and 260 m on a meteorological tower, respectively, for real-time characterization of submicron aerosol chemistry in Beijing from 22 August to 30 September 2015. Our results showed that regional emission controls were effective in reducing PM₁ levels by 57 and 50 % at ground level and 260 m, respectively, during the control period. Aerosol composition was also substantially different during and after the control period. While OA contributed the major fraction of PM₁ at both the ground site and 260 m (55 and 53 %, respectively) during the control period, its contribution was decreased to 40 % associated with an increase in SIA. These results illustrated a larger impact of emission controls on SIA reduction than OA, consistent with our previous findings during the APEC. The responses of POA and SOA to emission controls were investigated by positive matrix factorization analysis of OA. We found that the total POA decreased similarly to the total SOA at ground level (40 % vs. 42 %) and 260 m (35 % vs. 36 %) during the control period. However, the SOA composition at ground level had substantial changes during and after the control period. While the contribution of LO-OOA decreased from 52 to 35 %, MO-OOA increased from 13 to 30 %. It appears that photochemical production of less oxidized SOA was the dominant SOA formation mechanism during the control period, while aged SOA was more significant after the control period. Our results highlighted that regional emission controls not only reduce PM levels substantially, but likely affect SOA formation mechanisms as well. By comparing two polluted episodes with similar footprint regions during and after the control period, we found that regional emission controls reduced PM₁ levels by 44–45 % at different heights, and primary species had relatively more reductions (55–67 %) than secondary species (33–44 %) at ground level. The vertical differences for aerosol species between ground level and 260 m during and after the control period were also investigated. We found that $R_{260\text{m}/\text{Ground}}$ showed gradual decreases as a function of PM levels for most aerosol species during high loading periods ($> 60 \mu\text{g m}^{-3}$), indicating larger vertical gradients during more polluted episodes. In addition, $R_{260\text{m}/\text{Ground}}$ varied differently for primary and secondary species elucidating the different impacts of local emissions and regional transport on aerosol chemistry at different heights in the city.

Data availability. The data in this study are available from the authors upon request (sunyele@mail.iap.ac.cn).

The Supplement related to this article is available online at doi:10.5194/acp-17-3215-2017-supplement.

Competing interests. The authors declare that they have no conflict of interest.

Acknowledgements. This work was supported by the National Key Project of Basic Research (2014CB447900, 2013CB955801), the National Natural Science Foundation of China (41575120), the Special Fund for Environmental Protection Research in the Public Interest (201409001) and the Strategic Priority Research Program (B) of the Chinese Academy of Sciences (XDB05020501).

Edited by: J. Chen

Reviewed by: three anonymous referees

References

- Aiken, A. C., DeCarlo, P. F., and Jimenez, J. L.: Elemental analysis of organic species with electron ionization high-resolution mass spectrometry, *Anal. Chem.*, 79, 8350–8358, 2007.
- Aiken, A. C., Decarlo, P. F., Kroll, J. H., Worsnop, D. R., Huffman, J. A., Docherty, K. S., Ulbrich, I. M., Mohr, C., Kimmel, J. R., and Sueper, D.: O/C and OM/OC ratios of primary, secondary, and ambient organic aerosols with high-resolution time-of-flight aerosol mass spectrometry, *Environ. Sci. Technol.*, 42, 4478–4485, 2008.
- Aiken, A. C., Salcedo, D., Cubison, M. J., Huffman, J. A., DeCarlo, P. F., Ulbrich, I. M., Docherty, K. S., Sueper, D., Kimmel, J. R., Worsnop, D. R., Trimborn, A., Northway, M., Stone, E. A., Schauer, J. J., Volkamer, R. M., Fortner, E., de Foy, B., Wang, J., Laskin, A., Shutthanandan, V., Zheng, J., Zhang, R., Gaffney, J., Marley, N. A., Paredes-Miranda, G., Arnott, W. P., Molina, L. T., Sosa, G., and Jimenez, J. L.: Mexico City aerosol analysis during MILAGRO using high resolution aerosol mass spectrometry at the urban supersite (T0) – Part I: Fine particle composition and organic source apportionment, *Atmos. Chem. Phys.*, 9, 6633–6653, doi:10.5194/acp-9-6633-2009, 2009.
- Brown, S. S. and Stutz, J.: Nighttime radical observations and chemistry, *Chem. Soc. Rev.*, 41, 6405–6447, doi:10.1039/c2cs35181a, 2012.
- Canagaratna, M., Jayne, J., Jimenez, J., Allan, J., Alfarra, M., Zhang, Q., Onasch, T., Drewnick, F., Coe, H., and Middlebrook, A.: Chemical and microphysical characterization of ambient aerosols with the aerodyne aerosol mass spectrometer, *Mass Spectrom. Rev.*, 26, 185–222, 2007.
- Canagaratna, M. R., Jayne, J. T., Ghertner, D. A., Herndon, S., Shi, Q., Jimenez, J. L., Silva, P. J., Williams, P., Lanni, T., Drewnick, F., Demerjian, K. L., Kolb, C. E., and Worsnop, D. R.: Chase Studies of Particulate Emissions from in-use New York City Vehicles, *Aerosol Sci. Technol.*, 38, 555–573, doi:10.1080/02786820490465504, 2004.
- Canagaratna, M. R., Jimenez, J. L., Kroll, J. H., Chen, Q., Kessler, S. H., Massoli, P., Hildebrandt Ruiz, L., Fortner, E., Williams, L. R., Wilson, K. R., Surratt, J. D., Donahue, N. M., Jayne, J. T., and Worsnop, D. R.: Elemental ratio measurements of organic compounds using aerosol mass spectrometry: characterization, improved calibration, and implications, *Atmos. Chem. Phys.*, 15, 253–272, doi:10.5194/acp-15-253-2015, 2015.
- Carslaw, D. C. and Ropkins, K.: openair – An R package for air quality data analysis, *Environ. Modell. Softw.*, 27–28, 52–61, doi:10.1016/j.envsoft.2011.09.008, 2012.
- Chan, C. K. and Yao, X.: Air pollution in mega cities in China, *Atmos. Environ.*, 42, 1–42, 2008.
- Chen, C., Sun, Y. L., Xu, W. Q., Du, W., Zhou, L. B., Han, T. T., Wang, Q. Q., Fu, P. Q., Wang, Z. F., Gao, Z. Q., Zhang, Q., and Worsnop, D. R.: Characteristics and sources of submicron aerosols above the urban canopy (260 m) in Beijing, China, during the 2014 APEC summit, *Atmos. Chem. Phys.*, 15, 12879–12895, doi:10.5194/acp-15-12879-2015, 2015.
- DeCarlo, P. F., Kimmel, J. R., Trimborn, A., Northway, M. J., Jayne, J. T., Aiken, A. C., Gonin, M., Fuhrer, K., Horvath, T., and Docherty, K. S.: Field-deployable, high-resolution, time-of-flight aerosol mass spectrometer, *Anal. Chem.*, 78, 8281–8289, 2006.
- Du, W., Zhao, J., Wang, Y., Zhang, Y., Wang, Q., Xu, W., Chen, C., Han, T., Zhang, F., Li, Z., Fu, P., Li, J., Wang, Z., and Sun, Y.: Simultaneous measurements of particle number size distributions at ground level and 260 m on a meteorological tower in urban Beijing, China, *Atmos. Chem. Phys. Discuss.*, doi:10.5194/acp-2016-1064, in review, 2017.
- Elser, M., Huang, R.-J., Wolf, R., Slowik, J. G., Wang, Q., Canonaco, F., Li, G., Bozzetti, C., Daellenbach, K. R., Huang, Y., Zhang, R., Li, Z., Cao, J., Baltensperger, U., El-Haddad, I., and Prévôt, A. S. H.: New insights into PM_{2.5} chemical composition and sources in two major cities in China during extreme haze events using aerosol mass spectrometry, *Atmos. Chem. Phys.*, 16, 3207–3225, doi:10.5194/acp-16-3207-2016, 2016.
- Guo, S., Hu, M., Zamora, M. L., Peng, J., Shang, D., Zheng, J., Du, Z., Wu, Z., Shao, M., Zeng, L., Molina, M. J., and Zhang, R.: Elucidating severe urban haze formation in China, *P. Natl. Acad. Sci. USA*, 111, 17373–17378, doi:10.1073/pnas.1419604111, 2014.
- Han, S., Kondo, Y., Oshima, N., Takegawa, N., Miyazaki, Y., Hu, M., Lin, P., Deng, Z., Zhao, Y., Sugimoto, N., and Wu, Y.: Temporal variations of elemental carbon in Beijing, *J. Geophys. Res.*, 114, 1470–1478, doi:10.1029/2009jd012027, 2009.
- Han, T., Xu, W., Chen, C., Liu, X., Wang, Q., Li, J., Zhao, X., Du, W., Wang, Z., and Sun, Y.: Chemical apportionment of aerosol optical properties during the Asia-Pacific Economic Cooperation summit in Beijing, China, *J. Geophys. Res.-Atmos.*, 120, 12281–12295, doi:10.1002/2015jd023918, 2015.
- He, L.-Y., Lin, Y., Huang, X.-F., Guo, S., Xue, L., Su, Q., Hu, M., Luan, S.-J., and Zhang, Y.-H.: Characterization of high-resolution aerosol mass spectra of primary organic aerosol emissions from Chinese cooking and biomass burning, *Atmos. Chem. Phys.*, 10, 11535–11543, doi:10.5194/acp-10-11535-2010, 2010.
- Hu, W., Hu, M., Hu, W., Jimenez, J. L., Yuan, B., Chen, W., Wang, M., Wu, Y., Chen, C., and Wang, Z.: Chemical composition, sources, and aging process of submicron aerosols in Beijing: Contrast between summer and winter, *J. Geophys. Res.-Atmos.*, 120, 1955–1977, 2016a.
- Hu, W., Hu, M., Hu, W.-W., Niu, H., Zheng, J., Wu, Y., Chen, W., Chen, C., Li, L., Shao, M., Xie, S., and Zhang, Y.: Characterization of submicron aerosols influenced by biomass burning at a site in the Sichuan Basin, southwestern China,

- Atmos. Chem. Phys., 16, 13213–13230, doi:10.5194/acp-16-13213-2016, 2016b.
- Huang, R.-J., Zhang, Y., Bozzetti, C., Ho, K.-F., Cao, J.-J., Han, Y., Daellenbach, K. R., Slowik, J. G., Platt, S. M., Canonaco, F., Zotter, P., Wolf, R., Pieber, S. M., Bruns, E. A., Crippa, M., Ciarelli, G., Piazzalunga, A., Schwikowski, M., Abbaszade, G., Schnelle-Kreis, J., Zimmermann, R., An, Z., Szidat, S., Baltensperger, U., Haddad, I. E., and Prévôt, A. S. H.: High secondary aerosol contribution to particulate pollution during haze events in China, *Nature*, 514, 218–222, doi:10.1038/nature13774, 2014.
- Huang, X.-F., He, L.-Y., Hu, M., Canagaratna, M. R., Sun, Y., Zhang, Q., Zhu, T., Xue, L., Zeng, L.-W., Liu, X.-G., Zhang, Y.-H., Jayne, J. T., Ng, N. L., and Worsnop, D. R.: Highly time-resolved chemical characterization of atmospheric submicron particles during 2008 Beijing Olympic Games using an Aerodyne High-Resolution Aerosol Mass Spectrometer, *Atmos. Chem. Phys.*, 10, 8933–8945, doi:10.5194/acp-10-8933-2010, 2010.
- Huang, X.-F., He, L.-Y., Hu, M., Canagaratna, M. R., Kroll, J. H., Ng, N. L., Zhang, Y.-H., Lin, Y., Xue, L., Sun, T.-L., Liu, X.-G., Shao, M., Jayne, J. T., and Worsnop, D. R.: Characterization of submicron aerosols at a rural site in Pearl River Delta of China using an Aerodyne High-Resolution Aerosol Mass Spectrometer, *Atmos. Chem. Phys.*, 11, 1865–1877, doi:10.5194/acp-11-1865-2011, 2011.
- Huang, X.-F., He, L.-Y., Xue, L., Sun, T.-L., Zeng, L.-W., Gong, Z.-H., Hu, M., and Zhu, T.: Highly time-resolved chemical characterization of atmospheric fine particles during 2010 Shanghai World Expo, *Atmos. Chem. Phys.*, 12, 4897–4907, doi:10.5194/acp-12-4897-2012, 2012.
- Jayne, J. T., Leard, D. C., Zhang, X., Davidovits, P., Smith, K. A., Kolb, C. E., and Worsnop, D. R.: Development of an Aerosol Mass Spectrometer for Size and Composition Analysis of Submicron Particles, *Aerosol Sci. Technol.*, 33, 49–70, doi:10.1080/027868200410840, 2000.
- Jiang, Q., Sun, Y. L., Wang, Z., and Yin, Y.: Aerosol composition and sources during the Chinese Spring Festival: fireworks, secondary aerosol, and holiday effects, *Atmos. Chem. Phys.*, 15, 6023–6034, doi:10.5194/acp-15-6023-2015, 2015.
- Jimenez, J. L.: Ambient aerosol sampling using the Aerodyne Aerosol Mass Spectrometer, *J. Geophys. Res.*, 108, 447–457, doi:10.1029/2001jd001213, 2003.
- Lanz, V. A., Alfarra, M. R., Baltensperger, U., Buchmann, B., Hueglin, C., and Prévôt, A. S. H.: Source apportionment of submicron organic aerosols at an urban site by factor analytical modelling of aerosol mass spectra, *Atmos. Chem. Phys.*, 7, 1503–1522, doi:10.5194/acp-7-1503-2007, 2007.
- Li, H., Zhang, Q., Duan, F., Zheng, B., and He, K.: FDAT-MOS16 The “Parade Blue”: effects of short-term emission control on aerosol chemistry, *Faraday Discuss.*, 189, 317–335, doi:10.1039/C6FD00004E, 2016.
- Lide, D. R.: CRC handbook of chemistry and physics, CRC press, 1991.
- Liu, Q., Sun, Y., Hu, B., Liu, Z., Akio, S., and Wang, Y.: In situ measurement of PM₁ organic aerosol in Beijing winter using a high-resolution aerosol mass spectrometer, *Chinese Sci. Bull.*, 57, 819–826, doi:10.1007/s11434-011-4886-0, 2011.
- Liu, Z. R., Hu, B., Zhang, J. K., Yu, Y. C., and Wang, Y. S.: Characteristics of aerosol size distributions and chemical compositions during wintertime pollution episodes in Beijing, *Atmos. Res.*, 168, 1–12, doi:10.1016/j.atmosres.2015.08.013, 2016.
- Matthew, B. M., Middlebrook, A. M., and Onasch, T. B.: Collection Efficiencies in an Aerodyne Aerosol Mass Spectrometer as a Function of Particle Phase for Laboratory Generated Aerosols, *Aerosol Sci. Technol.*, 42, 884–898, doi:10.1080/02786820802356797, 2008.
- Middlebrook, A. M., Bahreini, R., Jimenez, J. L., and Canagaratna, M. R.: Evaluation of Composition-Dependent Collection Efficiencies for the Aerodyne Aerosol Mass Spectrometer using Field Data, *Aerosol Sci. Technol.*, 46, 258–271, doi:10.1080/02786826.2011.620041, 2012.
- Mohr, C., Huffman, J. A., Cubison, M. J., Aiken, A. C., Docherty, K. S., Kimmel, J. R., Ulbrich, I. M., Hannigan, M., and Jimenez, J. L.: Characterization of primary organic aerosol emissions from meat cooking, trash burning, and motor vehicles with high-resolution aerosol mass spectrometry and comparison with ambient and chamber observations, *Environ. Sci. Technol.*, 43, 2443–2449, 2009.
- Ng, N. L., Herndon, S. C., Trimborn, A., Canagaratna, M. R., Croteau, P. L., Onasch, T. B., Sueper, D., Worsnop, D. R., Zhang, Q., Sun, Y. L., and Jayne, J. T.: An Aerosol Chemical Speciation Monitor (ACSM) for Routine Monitoring of the Composition and Mass Concentrations of Ambient Aerosol, *Aerosol Sci. Technol.*, 45, 780–794, doi:10.1080/02786826.2011.560211, 2011.
- Paatero, P. and Tapper, U.: Positive matrix factorization: A non-factor model with optimal utilization of error estimates of data values, *Environmetrics*, 5, 111–126, 1994.
- Park, K., Kittelson, D. B., Zachariah, M. R., and McMurphy, P. H.: Measurement of inherent material density of nanoparticle agglomerates, *J. Nanopart. Res.*, 6, 267–272, 2004.
- Poulain, L., Birmili, W., Canonaco, F., Crippa, M., Wu, Z. J., Nordmann, S., Spindler, G., Prévôt, A. S. H., Wiedensohler, A., and Herrmann, H.: Chemical mass balance of 300 °C non-volatile particles at the tropospheric research site Melpitz, Germany, *Atmos. Chem. Phys.*, 14, 10145–10162, doi:10.5194/acp-14-10145-2014, 2014.
- Salcedo, D., Onasch, T. B., Dzepina, K., Canagaratna, M. R., Zhang, Q., Huffman, J. A., DeCarlo, P. F., Jayne, J. T., Mortimer, P., Worsnop, D. R., Kolb, C. E., Johnson, K. S., Zuberi, B., Marr, L. C., Volkamer, R., Molina, L. T., Molina, M. J., Cardenas, B., Bernabé, R. M., Márquez, C., Gaffney, J. S., Marley, N. A., Laskin, A., Shutthanandan, V., Xie, Y., Brune, W., Leshner, R., Shirley, T., and Jimenez, J. L.: Characterization of ambient aerosols in Mexico City during the MCMA-2003 campaign with Aerosol Mass Spectrometry: results from the CENICA Supersite, *Atmos. Chem. Phys.*, 6, 925–946, doi:10.5194/acp-6-925-2006, 2006.
- Skamarock, W. C., Klemp, J. B., Dudhia, J., Gill, D. O., Barker, D. M., Wang, W., and Powers, J. G.: A description of the advanced research WRF version 2, DTIC Document, 2005.
- Stohl, A., Forster, C., Frank, A., Seibert, P., and Wotawa, G.: Technical note: The Lagrangian particle dispersion model FLEXPART version 6.2, *Atmos. Chem. Phys.*, 5, 2461–2474, doi:10.5194/acp-5-2461-2005, 2005.
- Sun, J., Zhang, Q., Canagaratna, M. R., Zhang, Y., Ng, N. L., Sun, Y., Jayne, J. T., Zhang, X., Zhang, X., and Worsnop, D. R.: Highly time- and size-resolved characterization of

- submicron aerosol particles in Beijing using an Aerodyne Aerosol Mass Spectrometer, *Atmos. Environ.*, 44, 131–140, doi:10.1016/j.atmosenv.2009.03.020, 2010.
- Sun, Y., Zhuang, G., Tang, A. A., Wang, Y., and An, Z.: Chemical characteristics of PM_{2.5} and PM₁₀ in haze-fog episodes in Beijing, *Environ. Sci. Technol.*, 40, 3148–3155, 2006.
- Sun, Y., Wang, Z., Dong, H., Yang, T., Li, J., Pan, X., Chen, P., and Jayne, J. T.: Characterization of summer organic and inorganic aerosols in Beijing, China with an Aerosol Chemical Speciation Monitor, *Atmos. Environ.*, 51, 250–259, doi:10.1016/j.atmosenv.2012.01.013, 2012.
- Sun, Y., Wang, Z., Fu, P., Jiang, Q., Yang, T., Li, J., and Ge, X.: The impact of relative humidity on aerosol composition and evolution processes during wintertime in Beijing, China, *Atmos. Environ.*, 77, 927–934, doi:10.1016/j.atmosenv.2013.06.019, 2013.
- Sun, Y., Jiang, Q., Wang, Z., Fu, P., Li, J., Yang, T., and Yin, Y.: Investigation of the sources and evolution processes of severe haze pollution in Beijing in January 2013, *J. Geophys. Res.-Atmos.*, 119, 4380–4398, doi:10.1002/2014jd021641, 2014.
- Sun, Y., Du, W., Wang, Q., Zhang, Q., Chen, C., Chen, Y., Chen, Z., Fu, P., Wang, Z., Gao, Z., and Worsnop, D. R.: Real-Time Characterization of Aerosol Particle Composition above the Urban Canopy in Beijing: Insights into the Interactions between the Atmospheric Boundary Layer and Aerosol Chemistry, *Environ. Sci. Technol.*, 49, 11340–11347, doi:10.1021/acs.est.5b02373, 2015.
- Sun, Y., Wang, Z., Wild, O., Xu, W., Chen, C., Fu, P., Du, W., Zhou, L., Zhang, Q., and Han, T.: “APEC Blue”: Secondary Aerosol Reductions from Emission Controls in Beijing, *Sci. Rep.*, 6, 20668, 2016.
- Sun, Y.-L., Zhang, Q., Schwab, J. J., Demerjian, K. L., Chen, W.-N., Bae, M.-S., Hung, H.-M., Hogrefe, O., Frank, B., Rattigan, O. V., and Lin, Y.-C.: Characterization of the sources and processes of organic and inorganic aerosols in New York city with a high-resolution time-of-flight aerosol mass spectrometer, *Atmos. Chem. Phys.*, 11, 1581–1602, doi:10.5194/acp-11-1581-2011, 2011.
- Sun, Y. L., Wang, Z. F., Fu, P. Q., Yang, T., Jiang, Q., Dong, H. B., Li, J., and Jia, J. J.: Aerosol composition, sources and processes during wintertime in Beijing, China, *Atmos. Chem. Phys.*, 13, 4577–4592, doi:10.5194/acp-13-4577-2013, 2013.
- Sun, Y. L., Wang, Z. F., Du, W., Zhang, Q., Wang, Q. Q., Fu, P. Q., Pan, X. L., Li, J., Jayne, J., and Worsnop, D. R.: Long-term real-time measurements of aerosol particle composition in Beijing, China: seasonal variations, meteorological effects, and source analysis, *Atmos. Chem. Phys.*, 15, 10149–10165, doi:10.5194/acp-15-10149-2015, 2015.
- Tan, H., Xu, H., Wan, Q., Li, F., Deng, X., Chan, P., Xia, D., and Yin, Y.: Design and application of an unattended multifunctional H-TDMA system, *J. Atmos. Ocean. Technol.*, 30, 1136–1148, 2013.
- Tian, S., Pan, Y., Liu, Z., Wen, T., and Wang, Y.: Size-resolved aerosol chemical analysis of extreme haze pollution events during early 2013 in urban Beijing, China, *J. Hazard. Mater.*, 279, 452–460, doi:10.1016/j.jhazmat.2014.07.023, 2014.
- Turpin, B. J. and Lim, H.-J.: Species contributions to PM_{2.5} mass concentrations: Revisiting common assumptions for estimating organic mass, *Aerosol Sci. Technol.*, 35, 602–610, 2001.
- Ulbrich, I. M., Canagaratna, M. R., Zhang, Q., Worsnop, D. R., and Jimenez, J. L.: Interpretation of organic components from Positive Matrix Factorization of aerosol mass spectrometric data, *Atmos. Chem. Phys.*, 9, 2891–2918, doi:10.5194/acp-9-2891-2009, 2009.
- Wang, Q., Sun, Y., Jiang, Q., Du, W., Sun, C., Fu, P., and Wang, Z.: Chemical composition of aerosol particles and light extinction apportionment before and during the heating season in Beijing, China, *J. Geophys. Res.-Atmos.*, 120, 12708–12722, doi:10.1002/2015jd023871, 2015.
- Wang, Q., Huang, R.-J., Cao, J., Tie, X., Shen, Z., Zhao, S., Han, Y., Li, G., Li, Z., and Ni, H.: Contribution of regional transport to the black carbon aerosol during winter haze period in Beijing, *Atmos. Environ.*, 132, 11–18, 2016.
- Xu, J., Zhang, Q., Chen, M., Ge, X., Ren, J., and Qin, D.: Chemical composition, sources, and processes of urban aerosols during summertime in northwest China: insights from high-resolution aerosol mass spectrometry, *Atmos. Chem. Phys.*, 14, 12593–12611, doi:10.5194/acp-14-12593-2014, 2014.
- Xu, W. Q., Sun, Y. L., Chen, C., Du, W., Han, T. T., Wang, Q. Q., Fu, P. Q., Wang, Z. F., Zhao, X. J., Zhou, L. B., Ji, D. S., Wang, P. C., and Worsnop, D. R.: Aerosol composition, oxidation properties, and sources in Beijing: results from the 2014 Asia-Pacific Economic Cooperation summit study, *Atmos. Chem. Phys.*, 15, 13681–13698, doi:10.5194/acp-15-13681-2015, 2015.
- Zhang, J. K., Sun, Y., Liu, Z. R., Ji, D. S., Hu, B., Liu, Q., and Wang, Y. S.: Characterization of submicron aerosols during a month of serious pollution in Beijing, 2013, *Atmos. Chem. Phys.*, 14, 2887–2903, doi:10.5194/acp-14-2887-2014, 2014.
- Zhang, J. K., Wang, Y. S., Huang, X. J., Liu, Z. R., Ji, D. S., and Sun, Y.: Characterization of organic aerosols in Beijing using an aerodyne high-resolution aerosol mass spectrometer, *Adv. Atmos. Sci.*, 32, 877–888, doi:10.1007/s00376-014-4153-9, 2015.
- Zhang, Q., Canagaratna, M. R., Jayne, J. T., Worsnop, D. R., and Jimenez, J. L.: Time size chemical composition of submicron particles in Pittsburgh: Implications for aerosol sources and processes, *J. Geophys. Res.-Atmos.*, 110, 191–206, 2005.
- Zhang, R., Wang, G., Guo, S., Zamora, M. L., Ying, Q., Lin, Y., Wang, W., Hu, M., and Wang, Y.: Formation of Urban Fine Particulate Matter, *Chem. Rev.*, 115, 3803–3855, 2015.
- Zhang, Y. J., Tang, L. L., Wang, Z., Yu, H. X., Sun, Y. L., Liu, D., Qin, W., Canonaco, F., Prévôt, A. S. H., Zhang, H. L., and Zhou, H. C.: Insights into characteristics, sources, and evolution of submicron aerosols during harvest seasons in the Yangtze River delta region, China, *Atmos. Chem. Phys.*, 15, 1331–1349, doi:10.5194/acp-15-1331-2015, 2015.
- Zhao, X. J., Zhao, P. S., Xu, J., Meng, W., Pu, W. W., Dong, F., He, D., and Shi, Q. F.: Analysis of a winter regional haze event and its formation mechanism in the North China Plain, *Atmos. Chem. Phys.*, 13, 5685–5696, doi:10.5194/acp-13-5685-2013, 2013.